▌ Porphyrinoids

Syntheses, Properties, and Catalytic Activities of Metal(II) Complexes and Free Bases of Redox-Switchable 20π, 19π, and 18π 5,10,15,20-Tetraaryl-5,15-diazaporphyrinoids

Keisuke Sudoh,[b] Takaharu Satoh,[b] Toru Amaya,*[c] Ko Furukawa,*[d] Mao Minoura,[e] Haruyuki Nakano,[f] and Yoshihiro Matano*[a]

Abstract: In spite of significant advances in redox-active porphyrin-based materials and catalysts, little attention has been paid to 20π and 19π porphyrins because of their instability in air. Here we report the *meso*-modification of 5,10,15,20-tetraarylporphyrin with two nitrogen atoms, which led to redox-switchable 20π, 19π, and 18π 5,10,15,20-tetraaryl-5,15-diazaporphyrinoids (TADAPs). Three kinds of metal(II) complexes and free bases of TADAP were prepared by the metal-templated annulation of the corresponding metal-bis(dipyrrin) complexes. The inductive and resonance effects of the *meso*-nitrogen atoms on the aromatic, optical, electrochemical, and magnetic properties of the entire TADAP π-systems were assessed by using various spectroscopic measurements and density functional theory calcula-tions. The aromaticity and π–π* electronic transition ener-gies of the TADAPs varied considerably, and were shown to be dependent on the oxidation states of the π-systems. In contrast to the isoelectronic 5,10,15,20-tetraarylporphyrin derivatives, the 20π and 19π TADAPs were chemically stable under air. In particular, the 19π TADAP radical cations were extremely stable towards dioxygen, moisture, and silica gel. This reflected the low-lying singly occupied molecular orbi-tals of their π-systems and the efficient delocalization of their unshared electron spin. The capability of MgTADAP to catalyze aerobic biaryl formation from aryl Grignard reagents was demonstrated, which presumably involved a 19π/20π redox cycle.

[a] Prof. Dr. Y. Matano
Department of Chemistry, Faculty of Science
Niigata University, Nishi-ku, Niigata 950-2181 (Japan)
E-mail: matano@chem.sc.niigata-u.ac.jp

[b] K. Sudoh, T. Satoh
Department of Fundamental Sciences
Graduate School of Science and Technology
Niigata University, Nishi-ku, Niigata 950-2181 (Japan)

[c] Prof. Dr. T. Amaya
Department of Applied Chemistry, Graduate School of Engineering
Osaka University, Suita, Osaka 565-0871 (Japan)
E-mail: amaya@chem.eng.osaka-u.ac.jp

[d] Prof. Dr. K. Furukawa
Center for Coordination of Research Facilities
Institute for Research Promotion, Niigata University, Nishi-ku
Niigata 950-2181 (Japan)
E-mail: kou-f@chem.sc.niigata-u.ac.jp

[e] Prof. Dr. M. Minoura
Department of Chemistry, College of Science
Rikkyo University, Toshima-ku, Tokyo 171-8501 (Japan)

[f] Prof. Dr. H. Nakano
Department of Chemistry, Graduate School of Science
Kyushu University, Nishi-ku, Fukuoka 819-0395 (Japan)

Supporting information (experimental details and characterization data of new compounds) and the ORCID number(s) for the author(s) of this article are available under https://doi.org/10.1002/chem.201703664.

Introduction

Porphyrins are well known as redox-active macrocyclic ligands and 18π-electron aromatic molecules. The redox properties of porphyrins control a variety of electron/energy-transfer pro-cesses in nature and industry; therefore, there is considerable interest in the aromatic, optical, and magnetic properties of the resulting oxidized/reduced macrocyclic π-systems.[1, 2] One-electron and two-electron reductions of a neutral 18π porphy-rin ring produce the 19π radical anion and 20π dianion, re-spectively. In general, these anionic porphyrins are extremely air sensitive because of their high-lying SOMO and HOMO. Such sensitivity hampers their isolation and characterization in air. So far, three strategies for isolating 20π porphyrins in the neutral form have been reported: modification of the core ni-trogen atoms (core modification), metal complexation at the core, and peripheral substitution with appropriate functional groups.[3–13] Selected examples that have been prepared ac-cording to these strategies are shown in Figure 1. Vogel and co-workers reported the first examples of core-modified 20π porphyrins (isophlorins) **P 1** and tetraoxaisophlorin.[3] Similarly, N-alkyl-,[4] O-,[5] S-,[6] O,N-,[7] O,S-,[5] and P,S-containing[8] isophlor-ins have been reported by other groups. Vaid and co-workers synthesized the six-coordinate silicon(IV) and germanium(IV) complexes of 5,10,15,20-tetraphenylporphyrin (TPP) **P 2**[9] and phthalocyanine,[10] in which the N4-macrocycles were
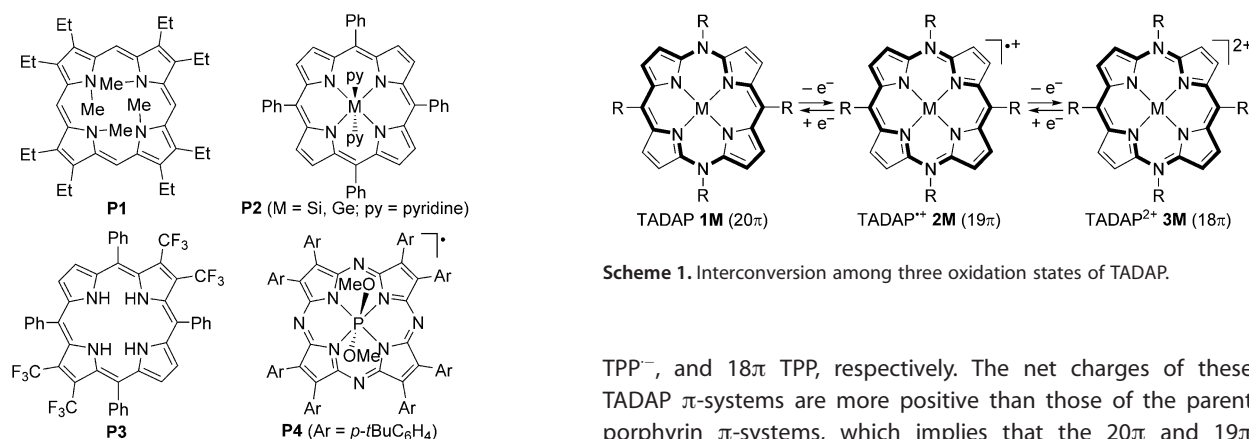
Figure 1. Selected examples of 20π and 19π porphyrins.

coordinated to the metal center as −4 anionic ligands with 20π electrons. Brothers et al. used the same strategy to obtain the 20π TPP-type porphyrin by inserting a diboron (B_2^{4+}) unit into the core.[11] We reported the combined use of core modification and metal complexation to obtain the air stable palladium(II) complex of P,S,N_2-isophlorin.[12] Chen et al. isolated the free base of isophlorin **P3** by appending four trifluoromethyl and four phenyl groups at the periphery of the porphyrin.[13] However, these approaches often caused severe distortion of the 20π framework because of steric repulsion of the substituents at the core or periphery. This distortion impeded a comprehensive understanding of the properties of the 20π/18π redox processes. Kobayashi et al. reported the first synthesis of an air stable 19π tetraazaporphyrin **P4**, which included a six-coordinate phosphorus(V) atom at the core;[14] to our knowledge there have been few reported air stable 19π porphyrins, and their potential as redox-active catalysts and materials has not yet been elucidated. Developing a conceptually new molecular design for precisely tuning the redox properties of porphyrin-based 19π- and 20π-systems is a challenge, both from a fundamental and an application perspective.

It is well known that the partial replacement of the *meso*-methine (CR; R=H, aryl, etc.) units of a porphyrin with nitrogen atoms lowers the porphyrin molecular symmetry, and stabilizes the HOMO and the LUMO energies of its π-system. For example, the redox properties of 5,15-diazaporphyrins (DAPs) differ substantially from those of their porphyrin counterparts;[15–17] DAPs are less readily oxidized and more readily reduced than porphyrins. In contrast, little attention has been paid to the *meso* modification of porphyrins with amine (NR) units. We envisioned that the replacement of two CR units at the 5 and 15 positions of TPP-type porphyrins with two NR units would be a promising strategy for obtaining redox-switchable 20π, 19π, and 18π azaporphyrins (Scheme 1). Our design concept is based on the idea that the unshared electron pairs of the two *meso*-N atoms would be involved in the π-system and alter its net charge for two electrons. Thus, 5,10,15,20-tetraaryl-5,15-diaza-5,15-dihydroporphyrin (TADAP, **1M**), its radical cation **2M** (TADAP[.+]), and its dication **3M** (TADAP[2+]) would be isoelectronic forms of 20π TPP[2−], 19π
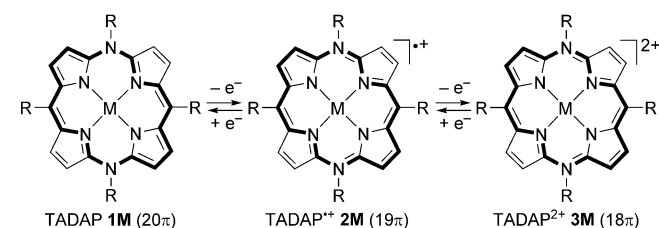
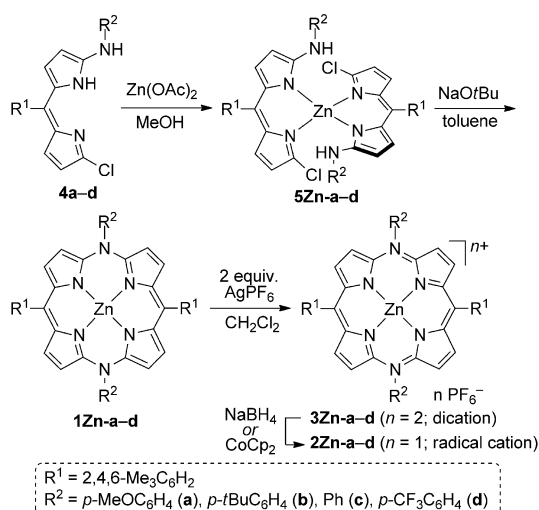**Scheme 1.** Interconversion among three oxidation states of TADAP.

TPP[.−], and 18π TPP, respectively. The net charges of these TADAP π-systems are more positive than those of the parent porphyrin π-systems, which implies that the 20π and 19π TADAP derivatives would be more resistant to oxidation than their porphyrin counterparts. This concept was demonstrated by us in the first syntheses of 20π, 19π, and 18π nickel(II) complexes of TADAP derivatives (NiTADAPs).[18] All NiTADAPs were isolable as air stable solids and exhibited reversible redox processes among the 20π/19π/18π oxidation states. Shinokubo and co-workers independently reported the synthesis of the nickel(II) complex and free base of the 20π 10,20-diaryl-5,15-diaza-5,15-dihydroporphyrin from the corresponding 18π DAPs.[19] However, these *meso*-NH derivatives readily underwent dehydrogenative oxidation in air to regenerate the parent DAPs.[20] These findings indicate that N-aryl groups in NiTADAPs provide substantial stability to the three π-systems, **1Ni**, **2Ni**, and **3Ni**. Encouraged by our preliminary results, we decided to investigate the effects of the central metals and *meso*-substituents on the fundamental properties of TADAP π-systems. We anticipated that a precisely designed TADAP could be used as a redox-active catalyst for the oxidative coupling of organomagnesium compounds under molecular oxygen as a terminal oxidant; this would be challenging owing to the possible side reaction of the organomagnesium compounds with molecular oxygen.[21] Herein, we report our comprehensive study of three kinds of metal(II) complexes and free bases of 20π, 19π, and 18π TADAPs. The syntheses and aromatic, optical, electrochemical, and magnetic properties of the TADAPs are discussed on the basis of both experimental and theoretical results. Preliminary results on the catalytic application of TADAP in the oxidative homocoupling of organomagnesium compounds are also reported.

## Results and Discussion

Synthesis

Scheme 2 illustrates the syntheses of zinc(II) complexes of TADAP derivatives (ZnTADAPs). The treatment of 3-chloro-5-arylamino-8-mesityldipyrrins **4a–d** (mesityl=2,4,6-trimethylphenyl) with half an equivalent of zinc(II) acetate afforded the corresponding zinc(II)-bis(dipyrrin) complexes **5Zn-a–d**. When the Zn-templated annulation reaction of complex **5Zn-a** was conducted with K_2CO_3 and DMF, which were used in the synthesis of NiTADAPs,[18] the desired 20π ZnTADAP **1Zn-a** was formed in low yield owing to the partial demetalation of the substrate

Scheme 2. Synthesis of ZnTADAPs.

$R^1 = 2,4,6\text{-}Me_3C_6H_2$
$R^2 = p\text{-}MeOC_6H_4$ (**a**), $p\text{-}tBuC_6H_4$ (**b**), Ph (**c**), $p\text{-}CF_3C_6H_4$ (**d**)

3Zn-a–d (n = 2; dication)
2Zn-a–d (n = 1; radical cation)

Scheme 3. Synthesis of CuTADAPs.

**3Cu-a,b,d** (n = 2)
2Cu-a,b,d (n = 1)

5Zn-a. Instead, when the reaction was carried out with NaOtBu and toluene, the expected annulation, namely an intramolecular double nucleophilic substitution reaction, of **5Zn-a** occurred smoothly to afford **1Zn-a**. Similarly, 20π ZnTADAPs **1Zn-b–d** were obtained from **5Zn-b–d**. The almost exclusive formation of **1Zn** from **5Zn** was confirmed by NMR spectroscopy and HRMS. However, **1Zn-a–d** were slowly oxidized in solution in the presence of air. Therefore, the crude products **1Zn-a–d** were oxidized directly with two equivalents of AgPF_6 to give 18π ZnTADAP^{2+} **3Zn-a–d**. Dicationic compounds **3Zn-a–d** were isolated as purple solids by recrystallization from CH_2Cl_2/Et_2O. The one-electron reduction of **3Zn-a–d** with NaBH_4 or bis(cyclopentadienyl)cobalt(II) (CoCp_2) at room temperature afforded the corresponding 19π ZnTADAP$^{·+}$ **2Zn-a–d**, which were isolated as greenish yellow solids by silica-gel column chromatography and subsequent recrystallization from $CH_2Cl_2/hexane$.

We next applied a metal-templated annulation method to synthesize copper(II) complexes of the TADAP derivatives (CuTADAPs). When dipyrrin **4b** was treated with half an equivalent of copper(II) acetate in $CH_2Cl_2/MeOH$, 19π CuTADAP$^{·+}$ **2Cu′-b** was unexpectedly obtained in a moderate yield instead of the anticipated copper(II)-bis(dipyrrin) complex **5Cu-b** (Scheme 3). The copper(II) salt most likely promoted the intramolecular N–C coupling of **5Cu-b**, but it also oxidized the resulting 20π CuTADAP. Indeed, when **4b** was treated with 1.2 equivalents of copper(II) acetate, we isolated **2Cu′-b** in a better yield. Similarly, 19πCuTADAP$^{·+}$ **2Cu′-a,d** were directly formed from dipyrrins **4a,d** after the reaction with copper(II) acetate. At this stage, the counter anions of **2Cu′** were not characterized, and **2Cu′** were reduced to 20π CuTADAPs **1Cu** by treatment with NaBH_4. Oxidation of **1Cu-a,b,d** with two equivalents of AgPF_6 afforded, after reprecipitation from CH_2Cl_2/Et_2O, the corresponding 18π CuTADAP^{2+} **3Cu-a,b,d**. Furthermore, the mixing of equimolar amounts of **1Cu** and **3Cu** in CH_2Cl_2 quantitatively produced 19π CuTADAP$^{·+}$ **2Cu-a,b,d** as hexafluorophosphates. In this antidisproportionation reaction, single-electron transfer from **1Cu** to **3Cu** occurred to form **2Cu** as a sole product.
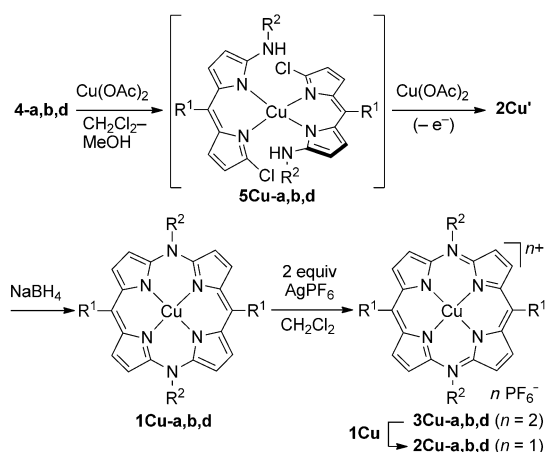
Free bases of TADAP derivatives (H_2TADAPs) were not afforded by the acidolysis of zinc(II) complexes **2Zn** and **3Zn**, which remained intact after prolonged treatment with CF_3CO_2H. Therefore, we used the Yorimitsu–Osuka procedure for the two-step transformation of metalloporphyrins into free bases via magnesium(II) porphyrins:[22] step one was exchange of the central metal from Ni/Zn/Cu/Ag to Mg by treatment with a Grignard reagent, and step two was acidolysis. Under our optimized reaction conditions, we obtained H_2TADAP from ZnTADAP **2Zn-a** in a moderate yield (Scheme 4). The addition of a large excess of phenylmagnesium bromide (THF solution) to a solution of **2Zn-a** in toluene rapidly effected a color change from yellow to red. The ^{1}H NMR and HRMS spectra of the reaction mixture were consistent with the formation of the 20π magnesium(II) complex of TADAP (MgTADAP) **1Mg-a**. However, this complex could not be isolated because of its extremely high sensitivity to air (see below). After the reaction mixture was stirred for ten minutes under a nitrogen atmosphere, it was treated with an excess of CF_3CO_2H, which cleaved the Mg–N bonds of **1Mg-a** to afford 20π H_2TADAP **1H_2-a** in 34% overall yield from **2Zn-a**. Alternatively, free base **1H_2-a** was

2H_2-a (n = 1)
3H_2-a (n = 2)
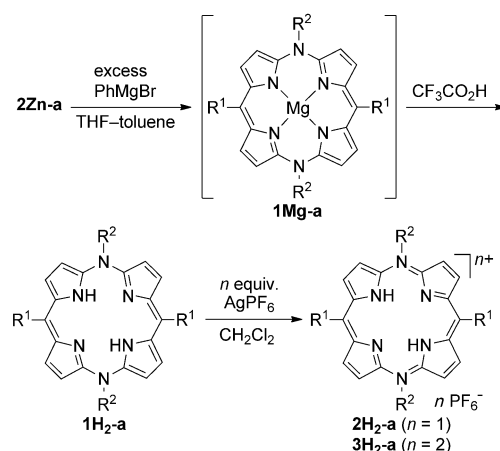
Scheme 4. Synthesis of H_2TADAPs.

prepared from **5 Zn-a** in a one-pot procedure via **1 Zn-a**, which underwent a Zn-to-Mg exchange reaction to give the transmetallated complex **1 Mg-a**. One-electron and two-electron oxidation reactions of **1 H₂-a** with AgPF₆ gave 19π H₂TADAP^{.+} **2 H₂-a** and 18π H₂TADAP^{2+} **3 H₂-a**, respectively. New NiTADAPs **1 Ni-a**, **2 Ni-a**, and **3 Ni-a** were prepared according to reported methods.[18] Notably, all of the radical cations **2 M** are rare examples of 19π porphyrins with a high stability towards dioxygen, moisture, and silica gel.

Characterization

MTADAPs (M=Zn, Cu, Ni, H₂) were characterized by NMR and IR spectroscopy, HRMS, and X-ray crystallography (for **1 Cu-b** and **2 Ni-a**). Intense peaks were detected in the HRMS spectra of MTADAPs **1 M**, **2 M**, and **3 M** that were consistent with $m/z =$ $[M]^+$, $[M-PF_6]^+$, and $[M-2(PF_6)]^{2+}$, respectively. In the ³¹P{¹H} NMR spectra of **2 M** and **3 M** (M=Zn, Ni), a characteristic septet from the hexafluorophosphate ion was observed at $\delta =$ $-141--146$ ppm ($J_{P-F} = 711-713$ Hz). The correlation between the ring-current effects in the ¹H NMR spectra and the aromaticity of the 20π and 18π MTADAPs (M=Zn, H₂) is discussed in the following section.

The crystal structures of two metal complexes **1 Cu-b** and **2 Ni-a** were elucidated by X-ray crystallography.[23] The copper center in **1 Cu-b** adopts a square-planar geometry, whereas the nickel center in **2 Ni-a** adopts an octahedral geometry with two oxygen atoms of the THF moiety as the axial ligands. Although the counter anion PF₆⁻ and the axial THF molecules of **2 Ni-a** showed positional disorder, the TADAP moiety was satisfactorily refined. As shown in Figure 2 and Figure S1 (see the Supporting Information), both **1 Cu-b** and **2 Ni-a** have very flat DAP π-planes with root-mean-square deviations (d_{rms}) of 0.029 and 0.044 Å, respectively. The meso-aryl groups are almost perpendicular to the DAP ring (dihedral angles are 74.0–86.5° for the 10,20-mesityl groups and 82.3–85.4° for the 5,15-aryl groups); this suggests that π-conjugation between the meso-aryl groups and the DAP ring is very small. The relatively short C1–N2 and C2–N2 bonds (average bond lengths = 1.381 and 1.371 Å for **1 Cu-b** and **2 Ni-a**, respectively) indicate that the unshared electron pairs in the p orbitals of the meso-N atoms are effectively conjugated with the π orbitals in the adjacent α-pyrrolic carbon atoms (see the Supporting Information, Table S1). The average Cu–N bond length of **1 Cu-b** (1.986 Å) is slightly longer than the average Ni–N bond length of **1 Ni-b** (1.945 Å),[18] which reflects the different covalent radii of Cu and Ni atoms.

Aromaticity

As mentioned above, the unshared electron pairs of the meso-N atoms of TADAP can be involved in the macrocyclic π-system. This implies that MTADAPs **1 M** and **3 M** are isoelectronic with the corresponding metal complexes of the 20π TPP dianion and 18π TPP, respectively. Taking these π-electron counts into consideration, the aromatic character of **1 M** and **3 M** was considered. Diatropic and paratropic ring-current ef-
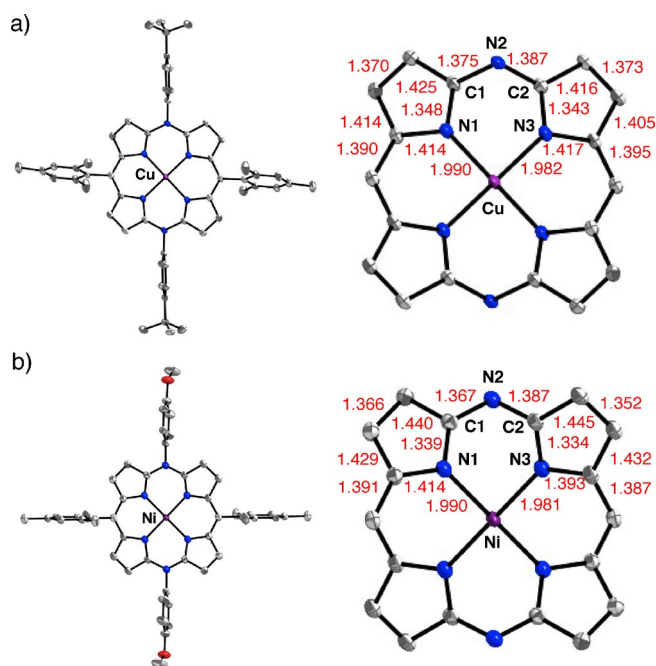
Figure 2. Top views (50 % probability ellipsoids) of a) **1 Cu-b** and b) **2 Ni-a** (a part of two independent crystals). Hydrogen atoms are omitted for clarity. For **2 Ni-a**, the counter ion PF₆⁻ and two axial THF ligands are also omitted. Bond lengths (Å), except the standard deviations (0.001–0.003 Å for **1 Cu-b**, 0.002–0.004 Å for **2 Ni-a**), are shown in red.
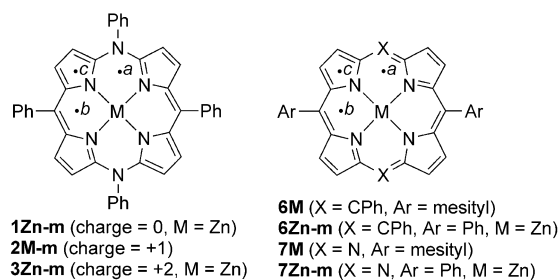
fects in the ¹H NMR spectra are a good index for evaluating aromaticity and antiaromaticity, respectively, in terms of a magnetic criterion. Representative ¹H NMR spectra are shown in Figure 3. The peripheral β protons (d and e) of **1 Zn-c** appeared at $\delta = 4.05$ and 2.81 ppm in C₆D₆, whereas those of **3 Zn-c** appeared at $\delta = 8.64$ and 8.25 ppm in CD₂Cl₂. These upfield and downfield shifts of the peripheral protons indicate that ZnTADAPs **1 Zn-c** and **3 Zn-c** receive considerable paratropic (20π) and diatropic (18π) ring currents, respectively. The ortho, meta, and para protons of the meso-aryl groups (c, f, g, and h) of **1 Zn-c** and **3 Zn-c** also receive the opposite ring-current effects to each other. Similar spectral features were observed for the other 20π/18π MTADAPs (M=Zn, Ni, H₂). The chemical shifts (in CDCl₃ or CD₂Cl₂) of the β protons of 18π MTADAPs **3 Zn** ($\delta = 8.64-8.54$, 8.27–8.20 ppm) and **3 H₂-a** ($\delta = 8.64$, 8.3 ppm) were shifted upfield compared with the corresponding chemical shifts of the 18π reference porphyrins **6 Zn** ($\delta = 8.89$, 8.78 ppm) and **6 H₂** ($\delta = 8.78$, 8.68 ppm).[24] In contrast, the β protons of 20π ZnTADAPs **1 Zn** ($\delta = 2.8-4.1$ ppm) were shifted downfield compared with those of a ZnTPP dianion ($\delta = -0.9$ ppm in [D₈]THF).[2d] These differences may be attributed to different charges and electron densities of the entire π-systems between **1 Zn**/**3 Zn** and the ZnTPP counterparts (20π dianion/18π neutral molecule). The ¹H NMR spectrum of free base **1 H₂-a** in C₆D₆ displayed a peak that represented the inner NH protons at $\delta = 24.87$ ppm (see the Supporting Information, Figure S2), which is close to the value reported for 10,20-dimesityl-5,15-diaza-5,15-dihydroporphyrin ($\delta = 24.5$ ppm in [D₈]THF).[19] The downfield shift of the NH protons of **3 H₂-a**
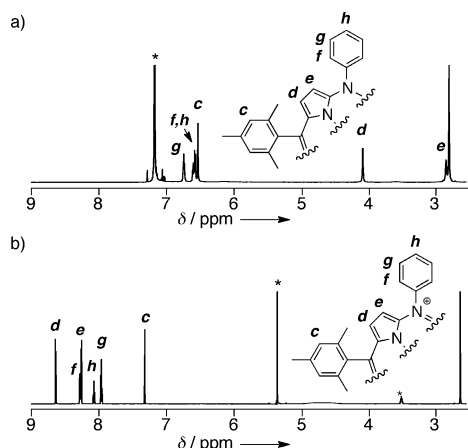
Figure 3. ¹H NMR spectra of a) **1Zn-c** in C_6D_6 and b) **3Zn-c** in CD_2Cl_2. Asterisks indicate residual solvent peaks.

($\delta = -0.54$ ppm) relative to those of **6H₂** ($\delta = -2.62$ ppm)[24] and **7H₂** ($\delta = -2.61$ ppm)[17b] may reflect a positive charge of the π-system in **3H₂-a**.

To gain a deeper insight into the ring-current effects of the TADAP π-systems, we calculated nuclear independent chemical shifts (NICS)[25] at three positions in the π-planes of the ZnTA-DAP models **1Zn-m** and **3Zn-m** (Figure 4). The NICS values at the midpoints between the two adjacent pyrrole rings (*a* and *b*) in **1Zn-m** were calculated to be +8.13 and +9.32 ppm, respectively, which indicates that there are global paratropic ring currents in its 20π-system. In contrast, the NICS value at the center of the pyrrole ring (*c*) in **1Zn-m** was −6.51 ppm, which implies that the pyrrole ring has local diatropic ring currents. The NICS values at the *a*, *b*, and *c* positions in the π-plane of **3Zn-m** were calculated to be −17.72, −17.11, and −7.06 ppm, respectively, which are apparently due to diatropic ring currents derived from the 18π-system. Based on ring-current effects, the DAP π-systems in **1Zn-m** and **3Zn-m** have substantial antiaromatic and aromatic character, respectively. The NICS values of **3Zn-m** were less negative than those of the porphyrin model **6Zn-m** ($\delta = -18.76$ and −9.26 ppm at *a* (=*b*) and *c*, respectively) and the DAP model **7Zn-m** ($\delta = -18.93$ and −19.22 ppm at *a* and *b*, respectively). This suggests that the macrocyclic ring-current effects of 18π ZnTADAP are slightly weaker than those of ZnTPP and ZnDAP.

1Zn-m (charge = 0, M = Zn)
2M-m (charge = +1)
3Zn-m (charge = +2, M = Zn)

6M (X = CPh, Ar = mesityl)
6Zn-m (X = CPh, Ar = Ph, M = Zn)
7M (X = N, Ar = mesityl)
7Zn-m (X = N, Ar = Ph, M = Zn)

Figure 4. MTADAP models (**1Zn-m**, **2M-m**, **3Zn-m**), porphyrin references and models (**6M**, **6Zn-m**), and DAP references and models (**7M**, **7Zn-m**).

Optical and redox properties

Table 1 summarizes the experimentally observed optical data for the MTADAPs and reference porphyrins/DAPs. The UV/Vis/NIR absorption spectra of the 5,15-*p*-anisyl-substituted derivatives **1M-a**, **2M-a**, and **3M-a** (M = Zn, Cu, Ni, H₂) are shown in Figure 5. Metal complexes **1M-a** exhibited two intense absorption bands with absorption maxima (λ_{max}) of 444–446 and 519–531 nm, whereas **3M-a** exhibited two intense bands with λ_{max} of 391–393 and 629–632 nm. The λ_{max} of the free bases **1H₂-a** (426 and 488 nm) and **3H₂-a** (390 and 645 nm) differed from those of their metal complexes, as is typically observed for porphyrins. The Q-like bands of **3M-c** (M = Zn, Ni) were largely red-shifted relative to the Q bands of **6M** ($\lambda_{max} = 526$–551 nm; M = Zn, Ni) and **7M** ($\lambda_{max} = 571$–584 nm; M = Zn, Ni). This indicates that the HOMO–LUMO gaps of the 18π MTADAPs are considerably smaller than those of the isoelectronic porphyrins and DAPs. The radical cations **2M-a** exhibited intense absorption

Table 1. Optical data for MTADAPs and references.	
Compound	λ_{abs} [nm] (log ε)[a]
1Zn-a	444 (n.d.), 519 (n.d.)
1Zn-b	445 (n.d.), 519 (n.d.)
1Zn-c	443 (n.d.), 518 (n.d.)
1Zn-d	443 (n.d.), 516 (n.d.)
1Cu-a	444 (5.05), 522 (4.87)
1Cu-b	444 (5.06), 523 (4.87)
1Cu-d	443 (5.09), 519 (4.94)
1Ni-a	446 (4.89), 531 (4.78)
1Ni-b	446 (4.96), 532 (4.85)[b]
1Ni-c	445 (4.94), 531 (4.81)[b]
1H₂-a	426 (4.80), 488 (4.53)
2Zn-a	384 (4.73), 448 (4.81), 890 (4.54)
2Zn-b	385 (4.79), 447 (4.90), 890 (4.63)
2Zn-c	384 (4.77), 445 (4.81), 894 (4.56)
2Zn-d	382 (4.79), 442 (4.85), 903 (4.55)
2Cu-a	384 (4.70), 444 (4.82), 871 (4.59)
2Cu-b	387 (4.66), 444 (4.88), 870 (4.59)
2Cu-d	384 (4.70), 440 (4.87), 879 (4.60)
2Ni-a	381 (4.63), 444 (4.78), 860 (4.47)
2Ni-b	384 (4.56), 444 (4.80), 860 (4.43)[b]
2H₂-a	375 (4.77), 449 (4.71), 888 (4.53)
3Zn-a	389 (4.76), 634 (4.63)
3Zn-b	388 (4.95), 634 (4.93)
3Zn-c	392 (4.66), 632 (4.65)
3Zn-d	391 (4.88), 634 (4.77)
3Cu-a	392 (4.95), 631 (4.85)
3Cu-b	391 (4.91), 630 (4.93)
3Cu-d	394 (4.85), 628 (4.72)
3Ni-a	393 (4.81), 629 (4.47)
3Ni-b	393 (4.82), 627 (4.55)[b]
3Ni-c	397 (4.78), 626 (4.51)[b]
3H₂-a	390 (n.d.), 645 (n.d.)
6Zn	421 (5.67), 551 (4.26)
6Ni	413 (5.29), 526 (4.15)[b]
7Zn	394 (4.92), 584 (4.86)[c]
7Cu	384 (4.98), 397 (4.97), 577 (4.94)[c]
7Ni	373 (4.79), 390 (4.89), 571 (4.78)[c]
7H₂	393 (5.11), 541 (4.51), 627 (4.62)[c]

[a] Measured in CH_2Cl_2; $\lambda_{max} > 350$ nm and log $\varepsilon > 4$ are listed; $R^2 = p$-$MeOC_6H_4$ (**a**), p-$tBuC_6H_4$ (**b**), Ph (**c**), p-$CF_3C_6H_4$ (**d**); n.d. = not determined. [b] Data from ref. [18]. [c] Data from ref. [17].
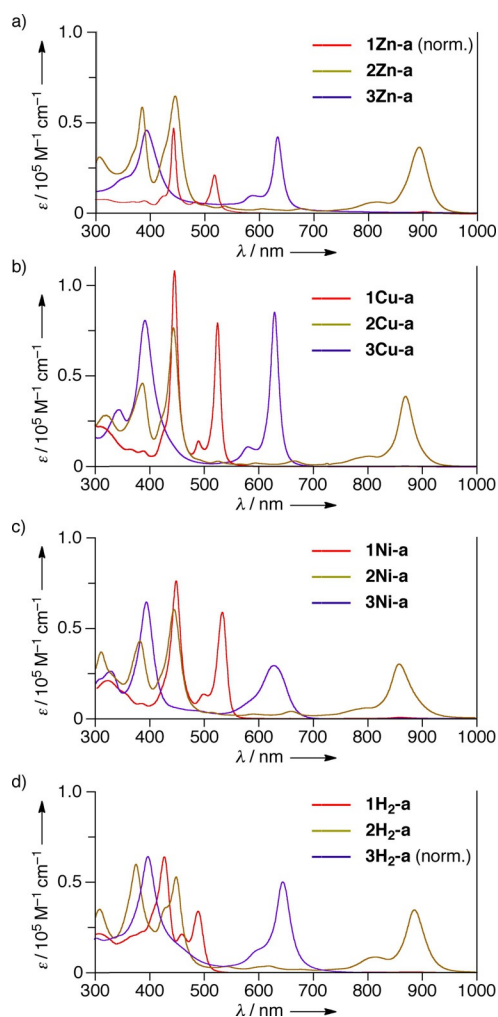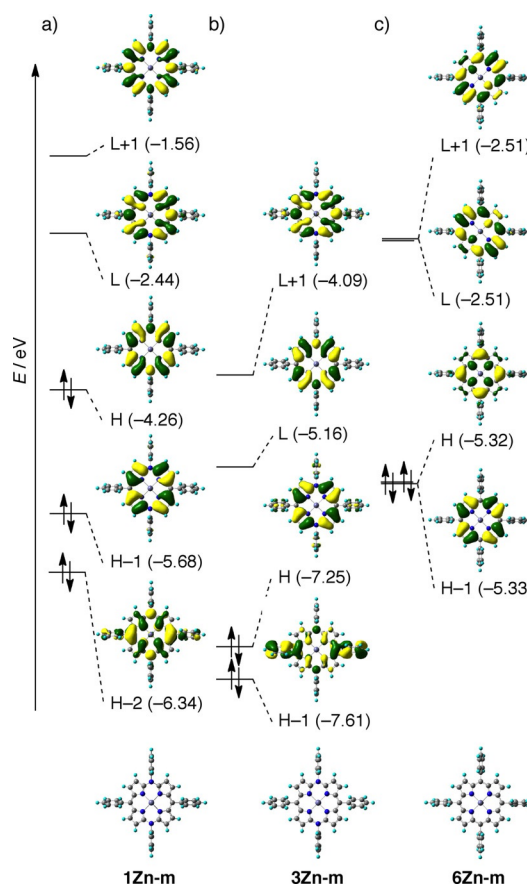
Figure 5. UV/Vis/NIR absorption spectra of MTADAPs (M = Zn) that bear *p*-anisyl groups: M = a) Zn, b) Cu, c) Ni, and d) H$_2$. Measured in CH$_2$Cl$_2$. The absorption spectra of **1Zn-a** and **3H$_2$-a** are normalized to those of **3Zn-a** and **1H$_2$-a**, respectively, at the absorption maxima.

Figure 6. Optimized structures and selected Kohn–Sham orbitals and their energies (eV) calculated by the DFT method with the solvent effect (PCM, CH$_2$Cl$_2$): a) **1Zn-m**, b) **3Zn-m**, and c) **6Zn-m**.

bands in the NIR region ($\lambda_{max} = 860$–890 nm) together with two bands in the UV/Vis region, which highlights the characteristic optical properties of their 19π-systems. In all three kinds of TADAPs, the *para* substituents of the *meso*-N-aryl groups exert only small influences on the λ_{max} values.

To understand the nature of π–π* electronic excitations of the TADAP π-systems, we carried out time-dependent density functional theory (TD-DFT) calculations on three zinc(II) complexes **1Zn-m**, **3Zn-m**, and **6Zn-m** (Figure 6 and Table 2; for the results on nickel(II) complexes, see ref. [18]). Both π-systems **1Zn-m** and **3Zn-m** have D_2 symmetry, and their HOMO/HOMO−1 and LUMO/LUMO+1 levels are nondegenerate because of the electronic effects of the two *meso*-N atoms. As shown in Figure 6, the electron distribution in the HOMO of **1Zn-m** largely corresponds to that of the LUMO of **3Zn-m**. This implies that the two electrons in the HOMO of **1Zn** are removed during the oxidation that leads to **3Zn**.

The orbital characteristics and energies of 18π ZnTADAP^{2+} **3Zn-m** differ considerably from those of ZnTPP **6Zn-m**, whose HOMO/HOMO−1 and LUMO/LUMO+1 are intrinsically degen-

erate and are located at high-lying energy levels because of the neutral D_4-symmetric π-system. From the results of the TD-DFT calculations, the bands of longest wavelength that were observed for **1Zn** were assigned to a combination of the HOMO-to-LUMO+1 and HOMO−1-to-LUMO excitations, whereas those observed for **3Zn** were assigned to the essential HOMO-to-LUMO excitation. The TD-DFT results also clarified that the HOMO-to-LUMO excitation of 20π ZnTADAP **1Zn-m** was symmetrically forbidden (oscillator strength ≈ 0).

The 18π ZnTADAP^{2+} **3Zn** and H$_2$TADAP^{2+} **3H$_2$-a** were weakly fluorescent in CH$_2$Cl$_2$ (see the Supporting Information, Figure S3). The optical HOMO–LUMO gaps of **3Zn-a** and **3H$_2$-a** (1.94 and 1.92 eV, respectively), as estimated from the intersections of the absorption and fluorescence spectra, were considerably smaller than those of the analogous porphyrin **6Zn** and MDAPs **7M** (M = Zn, H$_2$). Accordingly, the 18π TADAPs would be promising frameworks for cationic sensitizers that are capable of responding to long-wavelength visible light.

Redox potentials of the MTADAPs were measured by cyclic voltammetry in CH$_2$Cl$_2$ or THF, with Bu$_4$NPF$_6$ as a supporting electrolyte. Selected voltammograms are shown in Figure 7. Regardless of the starting materials (**1M**, **2M**, or **3M**), all the MTADAPs exhibited two reversible redox processes, which were attributed to 20π/19π and 19π/18π, in the range −0.7 to +1.0 V vs. Ag/Ag$^+$. For example, MTADAPs bearing the *p*-

Table 2. Excitation energies and oscillator strengths of models **1Zn-m**, **3Zn-m**, and **6Zn-m** calculated by the TD-DFT method.[a]

State	Excitation energy [eV/nm]	Oscillator strength (f)	Excitation	Weight [%]
1Zn-m				
2	2.41/515	0.166	HOMO→LUMO+1	75.5
			HOMO−1→LUMO	24.5
6	3.15/394	1.583	HOMO−1→LUMO	72.0
			HOMO→LUMO+1	23.6
11	3.40/365	0.149	HOMO−5→LUMO	61.0
			HOMO−2→LUMO	26.8
13	3.54/351	0.479	HOMO−2→LUMO	61.3
			HOMO−5→LUMO	32.0
3Zn-m				
2	2.01/616	0.393	HOMO→LUMO	90.3
16	3.07/404	0.599	HOMO−1→LUMO+1	89.5
17	3.19/389	0.305	HOMO−4→LUMO+1	61.0
20	3.37/368	1.241	HOMO−4→LUMO+1	35.3
			HOMO→LUMO	27.8
6Zn-m				
1	2.28/544	0.013	HOMO→LUMO+1	49.8
			HOMO−1→LUMO	49.8
3	3.12/398	1.619	HOMO−1→LUMO	49.4
			HOMO→LUMO	49.4

[a] B3LYP/6–311G(d,p) and Wachters–Hay(f) (PCM, CH_2Cl_2) at the optimized structures. Except for the lowest-energy excited state of **6Zn-m**, the states whose oscillator strengths are less than 0.1 are not included.
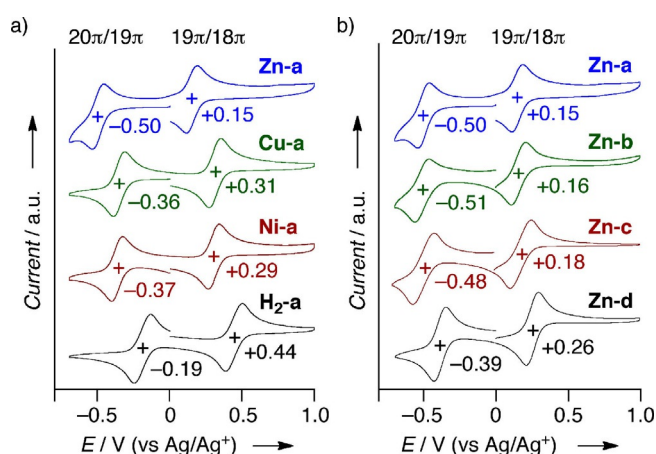
Figure 7. Cyclic voltammograms of a) MTADAPs that bear N-p-anisyl groups (M = Zn, Cu, Ni, H₂) and b) ZnTADAPs (a-d denote *para* substituents of the N-aryl groups). Measured in CH_2Cl_2 (from −0.7 to +1.0 V vs. Ag/Ag⁺); $Bu_4N^+PF_6^-$ (0.1 м) as a supporting electrolyte; Ag/Ag⁺ [AgNO₃ (MeCN)] as a reference electrode; scan rate = 60 mV s⁻¹.

anisyl groups were oxidized/reduced in two separate one-electron steps at −0.58 and +0.15 V for ZnTADAP, −0.36 and +0.31 V for CuTADAP, −0.37 and +0.29 V for NiTADAP, and −0.19 and +0.44 V for H₂TADAP (Figure 7a). Both the 20π/19π and 19π/18π redox processes of ZnTADAP occurred at more negative potentials than those of NiTADAP and CuTADAP, which reflects the smaller electronegativity of the zinc atom (1.65, Pauling scale) than those of copper (1.90) and nickel atoms (1.91). The more negative redox potentials observed for the 20π/19π process of ZnTADAP explains the relatively low stability of 20π ZnTADAP **1Zn** in air. However, the 20π/19π

redox processes of the MTADAPs occurred at much more positive potentials than those of the isoelectronic MTPP dianions ($E < -2$ V vs. Ag/Ag⁺). Therefore, it can be concluded that the high stability of **1M** arises from the neutral charge of their 20π-systems.[2d] It should also be noted that the electron-accepting ability of 18π MTADAP²⁺ **3M** is considerably higher than that of **6M** (i.e., $E(18π/19π) = +0.30$ V for **3Ni-c** and −1.69 V for **6Ni**, vs. Ag/Ag⁺). The 21π/20π and 20π/19π redox processes of **1Cu-b** in THF were observed at −1.88 and −0.33 V, respectively, vs. Ag/Ag⁺ (see the Supporting Information, Figure S4). From these values, the electrochemical HOMO–LUMO gap of **1Cu-b** was determined to be 1.55 eV.

The electronic effects of the *para* substituents of the N-aryl groups on the redox potentials of ZnTADAPs are displayed for comparison in Figure 7b. Introducing an electron-donating group (OMe, *t*Bu) slightly shifted the 20π/19π and 19π/18π processes towards more negative potentials ($\Delta E = -0.02$ to −0.03 V for **Zn-a,b** to **Zn-c**), whereas the introduction of an electron-withdrawing CF₃ group shifted them towards more positive potentials ($\Delta E = +0.08$ to +0.09 V for **Zn-d** to **Zn-c**). In all the metal complexes, the *para* substituents exerted small but clear influences on the HOMO and LUMO levels of the π-systems (Table 3).

Table 3. Redox Potentials for MTADAPs.[a]

M	a	b	c	d
Zn	−0.50, +0.15	−0.51, +0.16	−0.48, +0.18	−0.39, +0.26
Cu	−0.36, +0.31	−0.41, +0.27	n.p.	−0.29, +0.32
Ni	−0.37, +0.29	−0.39, +0.30	−0.37, +0.30	n.p.
H₂	−0.19, +0.44	n.p.	n.p.	n.p.

[a] Half-wave potentials (V vs. Ag/Ag⁺) measured by CV in CH_2Cl_2 with $Bu_4N^+PF_6^-$ (0.1 м); n.p. = not prepared.

Magnetic properties

As mentioned in the Introduction, there are currently few reported air-stable 19π porphyrins. To understand the key factors that provide the present 19π radical cations with their remarkable stability, we measured EPR spectra of MTADAPs **2Zn-a**–**d**, **2H₂-a**, **1Cu-a**, and **3Cu-a**. The EPR spectrum of **2Ni-c** has been reported previously.[18] As shown in Figure 8a, the spectrum of **2Zn-a** exhibits an EPR signal at $g = 2.0039$, which has a fine structure derived from two meso-¹⁴N and four β-¹H atoms. The calculated spin distribution of its model **2Zn-m** supported the observed fine structure (Figure 8b).

The other 19π ZnTADAPs **2Zn-b**–**d** exhibited similar EPR spectra, which illustrated the small electronic effects that their *para* substituents had on the electron spin distribution (see the Supporting Information, Figure S5). The free base **2H₂-a** exhibited an EPR spectrum at $g = 2.0023$, for which the fine structure was derived from meso-¹⁴N and β-¹H atoms (see the Supporting Information, Figure S6). Most importantly, the unshared electron spin of these 19π radical cations is efficiently delocalized over the entire DAP ring. The aryl groups attached to the meso-N/C atoms, which have moderate spin densities,
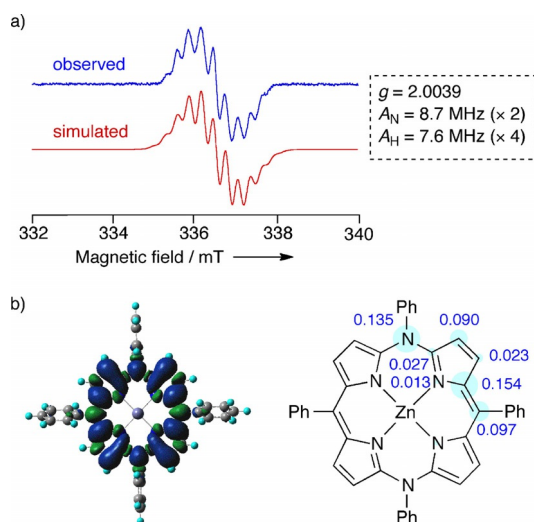
Figure 8. a) EPR spectra of **2Zn-a** observed in toluene (blue) and simulated (red). b) Spin-density distribution at the optimized structure (left) and spin densities at the DAP ring (right) of **2Zn-m**; calculated by the DFT method.

Figure 9. EPR spectra of a) **1Cu-a** and b) **3Cu-a** observed in CH_2Cl_2 at 30 K (blue) and simulated (red).

may also contribute to the stabilization of the π radicals by steric protection. The CuTADAPs **1Cu-a** and **3Cu-a** exhibited EPR signals that are characteristic of related copper(II) (diaza)-porphyrins.[26,27] Specifically, the fine structures that originated from the d^9 copper center and four core ^{14}N atoms (for **1Cu-a**) were observed at 30 K (Figure 9). These results clearly support the premise that the oxidation state (+2) of the copper center does not change during the redox conversion between two π-systems **1Cu** and **3Cu**.[28]

TADAP-catalyzed oxidative homocoupling reactions

As mentioned above, **2Zn-a** was transformed into **1Mg-a** by the reaction with excess PhMgBr, whereas **1Mg-a** was quickly converted to **2Mg-a** in air. These results indicate that 1) 19π MTADAP$^{\cdot+}$ can accept one electron from organomagnesium compounds to become the 20π MTADAP, and 2) 20π MgTA-DAP is readily oxidized by molecular oxygen to regenerate 19π MgTADAP$^{\cdot+}$.

With these reactivities in mind, we examined a catalytic oxidative homocoupling of PhMgBr under molecular oxygen to explore the possibility of MTADAP as a redox-active catalyst. The reaction progress was monitored by ^{1}H NMR and EPR spectroscopy (Figure 10) and MALDI-TOF MS spectrometry. Treatment of **2Zn-a** (19π) with PhMgBr in [D$_8$]THF under a nitrogen atmosphere at room temperature stoichiometrically afforded the desired coupling product, biphenyl, together with **1Zn-a** (20π; $\delta = 3.73$ and 2.74 ppm for β-H) and **1Mg-a** (20π; $\delta = 3.80$ and 2.84 ppm for β-H) (Figure 10a).[29] The addition of more PhMgBr induced the complete substitution of Zn^{II} to Mg^{II} in TADAP to give **1Mg-a** as the major TADAP product (Figure 10b). These observations clearly show that the oxidative homocoupling of PhMgBr is faster than the metal-exchange reaction. Introducing molecular oxygen to this mixture resulted in obvious changes in the ^{1}H NMR spectrum; specifically, we
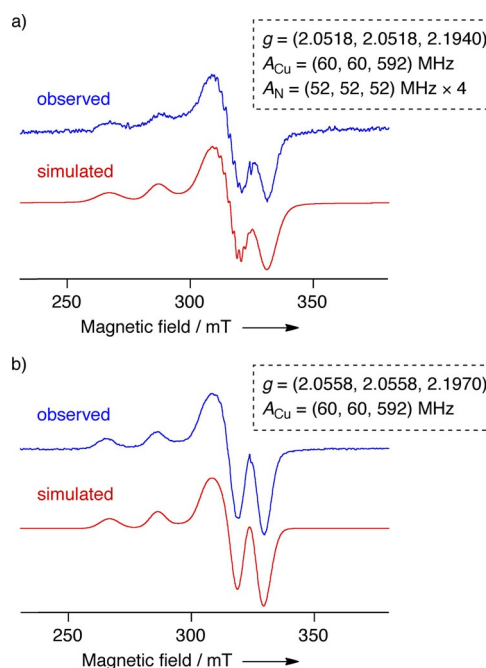
observed the disappearance of the peaks that corresponded to **1Mg-a**, and the growth of the peaks that were associated with biphenyl and a small amount of a phenol derivative (Figure 10c). In addition, the EPR and MALDI-TOF MS spectra of the resultant mixture showed the generation of **2Mg-a** (19π, $g = 2.003$). Again, a reaction sequence of the addition of PhMgBr followed by exposure to molecular oxygen was carried out. This resulted in similar observations in the ^{1}H NMR and EPR spectra (Figure 10d and e), which clearly demonstrates the catalytic cycle of 20π/19π MgTADAP (Scheme 5).[30]

Encouraged by this result, we also examined the oxidative homocoupling of 2-naphthylmagnesium bromide in the presence of 1 mol% of **2Zn-a** in THF. As expected, 2,2′-binaphthyl was obtained in 31% yield after 6 h, for which the catalytic turnover number was 31 (see the Supporting Information). Although there is ample room for improving the catalyst efficiency,[31] this is the first demonstration of diazaporphyrin as a redox-active catalyst in a C−C bond-forming redox reaction of organometallic reagents.

Conclusion

We investigated the synthesis and aromatic, optical, electrochemical, and magnetic properties of TADAPs in the three different oxidation states: 20π, 19π, and 18π. The metal-templated annulation method was effective for synthesizing the zinc(II) and copper(II) complexes, and the metal-exchange reaction was used to synthesize the free base. The redox potentials and chemical stabilities of the MTADAPs were strongly dependent on the central metals. The nickel(II) and copper(II) complexes were more resistant to oxidation than the zinc(II) counterparts, which reflects the difference in their electronega-
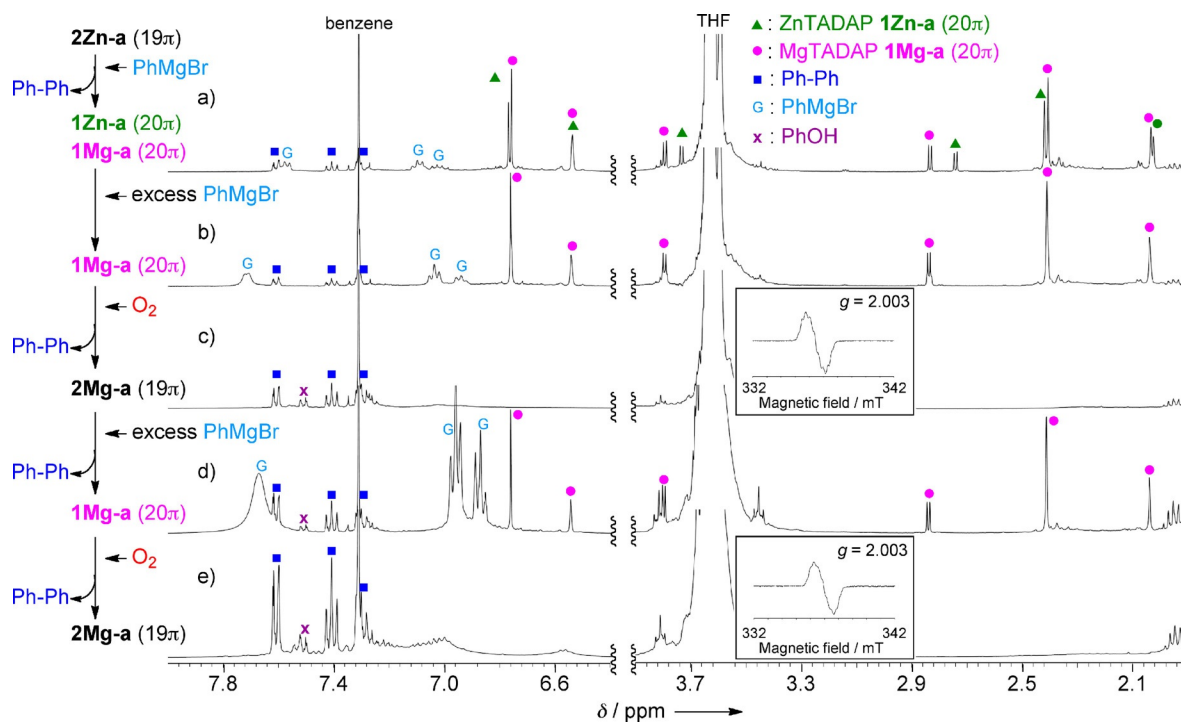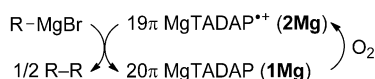
Figure 10. ^{1}H NMR and EPR spectra to follow the catalytic behavior of MTADAP during its oxidative homocoupling of PhMgBr in [D$_8$]THF.

Scheme 5. Plausible catalytic cycle for MgTADAP-catalyzed oxidative homocoupling reaction.

tivities. Because of the high electron affinity and resonance effects of nitrogen atoms at the *meso* positions, the 20π and 19π derivatives were resistant to air oxidation, whereas the 18π derivatives exhibited strong electron-accepting properties compared with the isoelectronic TPP derivatives. In particular, the 19π TADAP radical cations were extremely stable towards dioxygen, moisture, and silica gel, irrespective of the central metal atom. This stability is because the unshared electron spin can be efficiently delocalized in the cationic π-system. The antiaromatic and aromatic characters of 20π and 18π TADAPs, respectively, were confirmed by NMR spectroscopy and DFT calculations. These three π-systems showed quite different optical properties; their absorption bands ranged from 500 to 900 nm, which reflects their orbital characteristics. Notably, the redox processes among the 20π-, 19π-, and 18π-systems proceeded reversibly in one-electron steps. We have established the *meso* modification with nitrogen atoms as an alternative approach to intrinsically stabilize 20π and 19π porphyrin rings without the need to introduce any specific central metals or peripheral substituents. TADAPs can be used not only for the fundamental study of π-conjugated azamacrocycles but also for applied research on redox-active catalysts. This is demonstrated by the preliminary results on the oxidative homocou-

pling reactions of organomagnesium compounds. The reaction reported herein is the first example to show diazaporphyrin as a redox-active catalyst in a C−C bond-forming reaction of organometallic reagents. Further studies on developing new *meso*-modified azaporphyrinoids are underway.

Experimental Section

All melting points were recorded on a micro melting point apparatus and were uncorrected. NMR spectra were recorded on 700 MHz (Agilent) and/or 400 MHz (Agilent or JEOL JNM-ECP) spectrometers. The ^{1}H and ^{13}C chemical shifts are reported in ppm as relative values to the reference peak of tetramethylsilane (in CDCl$_3$ and CD$_2$Cl$_2$) or a solvent residual signal ($\delta_H = 7.16$ ppm in C$_6$D$_6$), and the ^{31}P chemical shifts are reported in ppm relative to the reference peak of H$_3$PO$_4$. High-resolution mass spectra were measured on a Thermo Fisher Scientific EXACTIVE spectrometer (electrospray-quadrupole), and MALDI-TOF mass spectra were recorded on a BRUKER AUTOFLEX III mass spectrometer. UV/Vis/NIR absorption spectra were measured on a JASCO V-530 spectrometer in the range of 300–1100 nm. The IR spectra were obtained on a PerkinElmer Spectrum GX spectrometer by using KBr pellets. Electrochemical redox potentials were measured by using a glassy carbon working electrode, a platinum wire counter electrode, and an Ag/Ag$^+$ reference electrode (0.01 M AgNO$_3$, 0.1 M Bu$_4$NPF$_6$ (MeCN)). UV/Vis fluorescence spectra were measured on an FP-8300 spectrometer. Fluorescence quantum yields were measured on a Hamamatsu Photonics Quantaurus-QY spectrometer. Thin-layer chromatography was performed with Kieselgel 60 F254, and preparative column chromatography was performed on Silica Gel 60 (spherical, neutral). All reactions were performed under an argon or nitrogen atmosphere, unless otherwise stated.

[1] 16π porphyrins: a) Y. Yamamoto, A. Yamamoto, S. Furuta, M. Horie, M. Kodama, W. Sato, K. − y. Akiba, S. Tsuzuki, T. Uchimaru, D. Hashizume, F. Iwasaki, *J. Am. Chem. Soc.* **2005**, 127, 14540–14541; b) J. A. Cissell, T. P. Vaid, G. P. A. Yap, *Org. Lett.* **2006**, 8, 2401–2404; c) Y. Yamamoto, Y. Hirata, M. Kodama, T. Yamaguchi, S. Matsukawa, K. Akiba, D. Hashizume, F. Iwasaki, A. Muranaka, M. Uchiyama, P. Chen, K. M. Kadish, N. Kobayashi, *J. Am. Chem. Soc.* **2010**, 132, 12627–12638; d) T. Kakui, S. Sugawara, Y. Hirata, S. Kojima, Y. Yamamoto, *Chem. Eur. J.* **2011**, 17, 7768–7771; e) S. Sugawara, M. Kodama, Y. Hirata, S. Kojima, Y. Yamamoto, *J. Porphyrins Phthalocyanines* **2011**, 15, 1326–1334; f) S. Hiramatsu, S. Sugawara, S. Kojima, Y. Yamamoto, *J. Porphyrins Phthalocyanines* **2013**, 17, 1183–1187.

[2] 20π porphyrin dianions: a) G. L. Closs, L. E. Closs, *J. Am. Chem. Soc.* **1963**, 85, 818–819; b) J. W. Buchler, L. Puppe, *Liebigs Ann. Chem.* **1970**, 740, 142–163; c) G. N. Sinyakov, A. M. Shul'ga, I. V. Filatov, G. P. Gurinovich, *Theor. Exp. Chem.* **1988**, 24, 37–44; d) R. Cosmo, C. Kautz, K. Meerholz, J. Heinze, K. Müllen, *Angew. Chem. Int. Ed. Engl.* **1989**, 28, 604–607; *Angew. Chem.* **1989**, 101, 638–640; e) K. M. Kadish, E. Van Caemelbecke, G. Royal, in *The Porphyrin Handbook Vol 8* (Eds.: K. M. Kadish, K. M. Smith, R. Guilard), Academic Press, San Diego, **2000**, pp. 1–114; f) B. K. Reddy, A. Basavarajappa, M. D. Ambhore, V. G. Anand, *Chem. Rev.* **2017**, 117, 3420–3443, and references therein.

[3] M. Pohl, H. Schmickler, J. Lex, E. Vogel, *Angew. Chem. Int. Ed. Engl.* **1991**, 30, 1693–1697; *Angew. Chem.* **1991**, 103, 1737–1741.

[4] a) J. Setsune, K. Kashihara, K. Wada, H. Shinozaki, *Chem. Lett.* **1999**, 28, 847–848; b) T. P. Vaid, *J. Am. Chem. Soc.* **2011**, 133, 15838–15841.

[5] a) J. S. Reddy, V. G. Anand, *J. Am. Chem. Soc.* **2008**, 130, 3718–3719; b) B. K. Reddy, S. C. Gadekar, V. G. Anand, *Chem. Commun.* **2015**, 51, 8276–8279.

[6] M. Kon-no, J. Mack, N. Kobayashi, M. Suenaga, K. Yoza, T. Shinmyozu, *Chem. Eur. J.* **2012**, 18, 13361–13371.

[7] S. P. Panchal, S. C. Gadekar, V. G. Anand, *Angew. Chem. Int. Ed.* **2016**, 55, 7797–7800; *Angew. Chem.* **2016**, 128, 7928–7931.

[8] a) T. Nakabuchi, M. Nakashima, S. Fujishige, H. Nakano, Y. Matano, H. Imahori, *J. Org. Chem.* **2010**, 75, 375–389; b) Y. Matano, T. Nakabuchi, H. Imahori, *Pure Appl. Chem.* **2010**, 82, 583–593.

[9] a) J. A. Cissell, T. P. Vaid, A. L. Rheingold, *J. Am. Chem. Soc.* **2005**, 127, 12212–12213; b) J. A. Cissell, T. P. Vaid, G. P. A. Yap, *J. Am. Chem. Soc.* **2007**, 129, 7841–7847.

[10] a) J. A. Cissell, T. P. Vaid, A. G. DiPasquale, A. L. Rheingold, *Inorg. Chem.* **2007**, 46, 7713–7715; b) E. W. Y. Wong, C. J. Walsby, T. Storr, D. B. Leznoff, *Inorg. Chem.* **2010**, 49, 3343–3350.

[11] a) A. Weiss, M. C. Hodgson, P. D. W. Boyd, W. Siebert, P. J. Brothers, *Chem. Eur. J.* **2007**, 13, 5982–5993; b) P. J. Brothers, *Chem. Commun.* **2008**, 2090–2102.

[12] a) Y. Matano, T. Nakabuchi, S. Fujishige, H. Nakano, H. Imahori, *J. Am. Chem. Soc.* **2008**, 130, 16446–16447; b) Y. Matano, H. Imahori, *Acc. Chem. Res.* **2009**, 42, 1193–1204.

[13] C. Liu, D.-M. Shen, Q.-Y. Chen, *J. Am. Chem. Soc.* **2007**, 129, 5814–5815.

[14] T. Yoshida, W. Zhou, T. Furuyama, D. B. Leznoff, N. Kobayashi, *J. Am. Chem. Soc.* **2015**, 137, 9258–9261.

[15] For selected reviews, see: a) K. Ishii, N. Kobayashi, in *The Porphyrin Handbook Vol 16* (Eds.: K. M. Kadish, K. M. Smith, R. Guilard), Academic Press, San Diego, **2003**, pp. 1–42; b) J. Mack, N. Kobayashi, *Chem. Rev.* **2011**, 111, 281–321; c) Y. Matano, *Chem. Rev.* **2017**, 117, 3138–3191.

[16] H. Ogata, T. Fukuda, K. Nakai, Y. Fujimura, S. Neya, P. A. Stuzhin, N. Kobayashi, *Eur. J. Inorg. Chem.* **2004**, 1621–1629.

[17] a) Y. Matano, T. Shibano, H. Nakano, H. Imahori, *Chem. Eur. J.* **2012**, 18, 6208–6216; b) Y. Matano, T. Shibano, H. Nakano, Y. Kimura, H. Imahori, *Inorg. Chem.* **2012**, 51, 12879–12890.

[18] T. Satoh, M. Minoura, H. Nakano, K. Furukawa, Y. Matano, *Angew. Chem. Int. Ed.* **2016**, 55, 2235–2238; *Angew. Chem.* **2016**, 128, 2275–2278.

[19] M. Horie, Y. Hayashi, S. Yamaguchi, H. Shinokubo, *Chem. Eur. J.* **2012**, 18, 5919–5923.

[20] A. Yamaji, H. Tsurugi, Y. Miyake, K. Mashima, H. Shinokubo, *Chem. Eur. J.* **2016**, 22, 3956–3961.

[21] a) A. Krasovskiy, A. Tishkov, V. del Amo, H. Mayr, P. Knochel, *Angew. Chem. Int. Ed.* **2006**, 45, 5010–5014; *Angew. Chem.* **2006**, 118, 5132–5136; b) G. Cahiez, A. Moyeux, J. Buendia, C. Duplais, *J. Am. Chem. Soc.* **2007**, 129, 13788–13789; c) W. Liu, A. Lei, *Tetrahedron Lett.* **2008**, 49, 610–613; d) M. S. Maji, T. Pfeifer, A. Studer, *Angew. Chem. Int. Ed.* **2008**, 47, 9547–9550; *Angew. Chem.* **2008**, 120, 9690–9692; e) S.-K. Hua, Q.-P. Hu, J. Ren, B.-B. Zeng, *Synthesis* **2013**, 45, 518–526; f) T. Amaya, R. Suzuki, T. Hirao, *Chem. Eur. J.* **2014**, 20, 653–656; g) T. Korenaga, K. Nitatori, H. Muraoka, S. Ogawa, K. Shimada, *Org. Lett.* **2015**, 17, 5500–5503; h) S. Murarka, J. Möbus, G. Erker, C. Mück-Lichtenfeld, A. Studer, *Org. Biomol. Chem.* **2015**, 13, 2762–2767; i) T. Amaya, R. Suzuki, T. Hirao, *Chem. Commun.* **2016**, 52, 7790–7793.

[22] K. Murakami, Y. Yamamoto, H. Yorimitsu, A. Osuka, *Chem. Eur. J.* **2013**, 19, 9123–9126.

[23] The X-ray diffraction data for several crystals of **2M** and **3M** (M = Zn, Cu) indicated that their DAP rings are very flat; however, these data could not be fully refined to a publishable level because of uncertain loss or positional disorder of the solvent molecules that were included.

[24] B. J. Littler, Y. Ciringh, J. S. Lindsey, *J. Org. Chem.* **1999**, 64, 2864–2872.

[25] P. v. R. Schleyer, C. Maerker, A. Dransfeld, H. Jiao, N. J. R. van Eikema Hommes, *J. Am. Chem. Soc.* **1996**, 118, 6317–6318.

[26] S. P. Greiner, D. L. Rowlands, R. W. Kreilick, *J. Phys. Chem.* **1992**, 96, 9132–9139.

[27] Y. Matano, D. Fujii, T. Shibano, K. Furukawa, T. Higashino, H. Nakano, H. Imahori, *Chem. Eur. J.* **2014**, 20, 3342–3349.

[28] No X- and W-band EPR signals were observed for copper(II) complex **2Cu-a** at room temperature and 20 K, respectively, probably because the large zero-field splitting interaction between the d⁹ copper center and TADAP π-radical induced a significant line-broadening. In addition, no NMR signal was observed for **2Cu-a** at room temperature, which may suggest a contribution of the triplet ground state. However, the detailed discussion on the spin state of 19π CuTADAP is beyond the scope of the present paper and will be reported elsewhere.

[29] In the case of 1,4-benzoquinone as a typical two-electron oxidant, the oxidative coupling product of PhMgBr was not obtained in THF. Instead, PhMgBr attacked the carbonyl groups to give the 1,2-addition adduct.

[30] The mechanism of the reaction is not clear at present. According to the previous reports,[21a,h] the homocoupling reaction may take place through a stepwise electron transfer: 1) electron transfer from PhMgBr to **2Mg-a** (or **2Zn-a**) (19π) to form a kind of phenyl radical species, 2) addition of PhMgBr to the radical species to give Ph–Ph radical anion species, and 3) electron transfer from the radical anion species to another molecule of **2Mg-a** (or **2Zn-a**) (19π) to afford Ph–Ph.

[31] The MALDI-TOF MS spectrum of the crude mixture in the ¹H NMR experiments shown in Figure 10 indicated the formation of a small amount of the adduct formed from the Grignard reagent and TADAP, although the main peak exhibited the desired 19π MgTADAP **2Mg-a**. This might cause a decrease of the catalyst efficiency.